electronics

MDPI

Article

A Markov State-Transition-Aware Event-Driven Compensation Method for All-Digital Transmitters

Mingqi Wang [1,2], Xingyu Zhou [1,2], Lei Zhu [2], Zhihu Wei [2] and Zhang Chen [2,*]

[1] College of Electronic and Information Engineering, Nanjing University of Information Science and Technology, Nanjing 210044, China; 202412491637@nuist.edu.cn (M.W.); 202512491089@nuist.edu.cn (X.Z.)
[2] Sixty-Third Research Institute, National University of Defense Technology, Nanjing 210007, China; zhuleidz@163.com (L.Z.); plawzh@163.com (Z.W.)
* Correspondence: darp@nudt.edu.cn; Tel.: +86-15850516085

Abstract

All-digital transmitters (ADTx) synthesize radio-frequency (RF) waveforms through coordinated binary switching, where delay mismatch, parasitic effects, and dynamic response differences among switching paths introduce transient distortions with strong state- and transition-path dependence. Conventional waveform-based digital predistortion (DPD) treats the ADTx as an equivalent nonlinear system and lacks awareness of internal state transitions, limiting targeted compensation of high-risk events. This paper proposes an adaptive state-transition compensation method based on four-dimensional binary state-vector Markov modeling and event-driven local predistortion. The four switching states of a five-level ADTx are encoded as a binary vector, and a first-order Markov model with 16 states characterizes the state evolution. By jointly considering transition probability, state-change magnitude, and steady-state probability, a transition-importance matrix quantifies all 256 transition paths and identifies the effective ones, for which a path-specific finite impulse response (FIR) compensation kernel library is developed. An event-driven mechanism activates the corresponding kernel only at transition events, enabling localized compensation of transient distortions. Simulations show an adjacent channel power ratio (ACPR) improvement of 11.5 dB and an error vector magnitude (EVM) reduction of 4.8% over the uncompensated system, while only approximately 19% of transition events require online compensation, substantially reducing real-time computational overhead.

Keywords: multi-level all-digital transmitter; state vector; Markov state-transition model; transition-path-aware compensation; event-driven digital predistortion

Check for updates

Academic Editor: Youngkyun Cho

Received: 20 September 2026
Revised: 22 October 2026
Accepted: 22 October 2026
Published: 26 October 2026

Copyright: © 2026 by the authors. Licensee MDPI, Basel, Switzerland. This article is an open access article distributed under the terms and conditions of the Creative Commons Attribution (CC BY) license.

1. Introduction

Driven by 6G communications, wide-band software-defined radio (SDR) [1], and large-scale array systems, future wireless transmitters must simultaneously achieve ultra-wide bandwidth, high efficiency, high linearity, and high integration. All-digital transmitters (ADTx), which directly perform signal generation, upconversion, and power combining through digitally controlled switching stages, offer a compact, programmable, and CMOS-scalable alternative to analog mixers, filters, and linear power amplifiers [2–7]. Existing ADTx architectures include quadrature, polar, and outphasing types, with RF pulse-width modulation (RF-PWM) and digital delay techniques enabling direct time-domain control of amplitude, phase, and spectral characteristics [8–10]. Among them, multi-level architectures improve waveform-reconstruction accuracy by increasing the number of discrete

output states [11,12], Low-cost all-digital transmitter implementations have also been investigated [13], while outphasing-based implementations synthesize amplitude-varying signals from constant-envelope branches [14–17]. The five-level RF-PWM outphasing ADTx considered in this work coordinates multiple binary branches to achieve fine waveform representation while retaining high switching efficiency [3,18], and thus serves as a representative platform for investigating state- and transition-dependent nonlinearities in multi-level ADTx.

Unlike continuous-time RF power amplifiers, a multi-level ADTx constructs its output waveform through the coordinated evolution of multiple binary state variables. Practical nonidealities such as propagation-delay mismatch, parasitic charging and discharging, driver-path variations, and inter-channel timing skew introduce pulse-amplitude imbalance, delay distortion, overshoot and edge distortion [18–20]. And previous studies have shown that the transient response is dominated by the dynamic behavior of the constituent branches. Crucially, since each output level is jointly determined by multiple binary state combinations, the same output-level transition may arise from different underlying state transitions with distinct transient responses [21]. The resulting distortion is therefore both state-dependent and transition-path-dependent, which conventional global behavioral models fail to capture. Moreover, directly modeling state histories suffers from exponential state-space growth 2^{nL} histories for n binary variables with memory length L, and since transient distortion is concentrated around transition events. Conventional digital predistortion (DPD) approaches include Volterra-based, memory-polynomial, conditional-memory, and model-switching structures [22–27]. Digital predistortion and phase predistortion techniques have also been investigated for outphasing power amplifiers [14–17]. However, these approaches do not explicitly exploit the underlying multi-channel binary state-transition paths. Finite-state Markov models provide an effective framework for characterizing the statistical evolution of discrete-state sequences [28–30]. Nevertheless, their application to transition-path-dependent transient distortion compensation in multi-level ADTx remains insufficiently explored.

To address these challenges, this paper proposes an adaptive transition-compensation method based on binary state-vector Markov transition awareness and event-driven local predistortion. A first-order Markov model is established over the binary state space to characterize the statistical evolution of the switching-state sequence. Based on this model, a state-transition path importance matrix is constructed by jointly considering transition probability, state-change characteristics, and state residence probability. This matrix is then used to identify critical transition paths for transient-distortion compensation. Path-specific FIR compensation kernels are then designed for the important paths and activated only when the corresponding transition event is detected, concentrating compensation within transient regions while avoiding unnecessary predistortion during steady-state intervals. The main contributions are as follows. (1) A binary state-vector Markov modeling and transition-path importance evaluation method for multi-level ADTx, which identifies the transition paths most relevant to transient-distortion compensation by exploiting the statistics of the underlying binary state sequence. (2) An event-driven local compensation method based on a path-specific FIR kernel library, which triggers compensation only upon state-transition events and selects the kernel according to the identified transition path, thereby reducing real-time computational overhead.

The remainder of this paper is organized as follows. Section 2 presents the multi-level ADTx architecture and transition-induced distortion. Section 3 introduces the proposed Markov state-aware adaptive transition compensation method. Section 4 evaluates its performance in terms of error vector magnitude (EVM), adjacent channel power ratio (ACPR) and computational complexity. Finally, Section 5 concludes the paper.

2. Multi-Level ADTx System Model and Transition-Induced Distortion Analysis

2.1. Multi-Level ADTx Architecture and Markov State-Transition Modeling

Multi-level ADTx directly synthesize RF waveforms through discrete combinations of multiple binary power branches. ADTx drive switching power devices with digitally generated PWM signals, offering high power efficiency and scalability [7,9,11].

In this paper, a five-level outphasing ADTx architecture is considered, and its signal generation process is illustrated in Figure 1. In this study, the five-level outphasing ADTx architecture is adopted from the established principles of RF-PWM outphasing and multilevel transmitter techniques reported [3,11]. Figure 1 presents a schematic diagram independently drawn by the authors to illustrate the signal generation process of the adopted architecture. The transmitter architecture itself is not a new contribution of this work. Instead, the proposed method focuses on Markov state-transition-aware event-driven compensation to mitigate transient distortions associated with the internal switching-state transitions. The input complex baseband signal is expressed as:

$$x(t) = A(t)e^{j\phi(t)}, \tag{1}$$

where $A(t)$ and $\Phi(t)$ denote the signal envelope and phase, respectively. After amplitude-phase decomposition, the system generates four outphasing PWM control signals.

$$x_n(t) \in \{0,1\},\ n = 1,2,3,4. \tag{2}$$

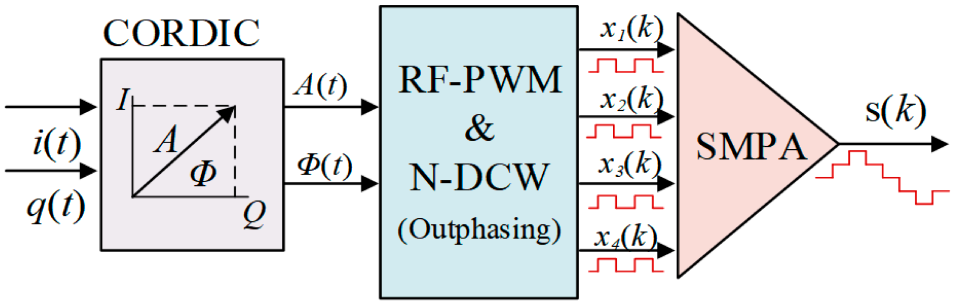


Figure 1. Schematic architecture of the five-level outphasing ADTx based on existing RF-PWM and multilevel transmitter techniques [3,18].

The four binary control signals are applied to their corresponding parallel power branches. Under ideal conditions, the outputs of the four branches are combined through the RF power-combining network to form a five-level discrete output waveform. For an equal-weight configuration, the output levels can be expressed as:

$$s(k) = \frac{1}{2}\sum_{n=1}^{4} x_n(k). \tag{3}$$

Accordingly, the output level of the system is given by $s(k) \in \{-2, -1, 0, 1, 2\}$. Equation (3) shows that the output level of the multi-level ADTx is jointly determined by the discrete state combinations of multiple branches. However, unlike conventional multi-level modulators, the actual transient response of a multi-level ADTx is not determined solely by the output level, but is also influenced by the discrete state combination of the branches that produces the corresponding output level. To characterize the dynamic interactions

among the multiple power-switching branches, the state vector at the k-th discrete sampling instant is defined as:

$$X_k = [x_1(k), x_2(k), x_3(k), x_4(k)]^T, x_n(k) \in \{0,1\}, \quad (4)$$

where $x_n(k)$ denotes the binary state of the n-th branch at the k-th sampling instant. And $X_k \in X$ represents the corresponding four-dimensional joint switching-state vector.

Since the ADTx consists of four binary switching branches, the system theoretically has $2^4 = 16$ possible joint states. The finite state space is denoted by $X = \{X_1, X_2, \ldots, X_{16}\}$. where X_i represents the i-th possible switching-state configuration. Throughout this paper, X_k denotes the joint state observed at sampling instant k, whereas X_i and X_j denote the initial and final states of a transition path T_{ij}: $X_i \rightarrow X_j$.

Although different joint switching states may correspond to the same output level, their binary configurations and subsequent state transitions may differ. Therefore, the output level $s(k)$ alone cannot fully characterize the transient nonlinearities associated with the internal switching-state variations. In contrast, the binary state vector retains the state information of individual switching branches, enabling a more detailed characterization of state-dependent transient behavior.

To characterize the temporal evolution of the switching states, a first-order Markov model is adopted. The state sequence exhibits temporal correlation because the switching operations are governed by the modulation process and the relationships among the carrier phases. Under the first-order Markov assumption, the probability distribution of the next state $x(k + 1)$ depends only on the current state $x(k)$, rather than the complete history of preceding states [29,30]:

$$\Pr\{X(k+1) \mid X(k), X(k-1), \ldots, X(0)\} = \Pr\{X(k+1) \mid X(k)\}. \quad (5)$$

This assumption does not imply that the physical transient response of the ADTx is inherently memoryless or lacks long-term memory. Rather, at the statistical state-modeling level, it assumes that the current discrete state provides a sufficient representation for predicting the next state. The dynamic effects associated with practical transient distortions, including amplitude errors, delay mismatch, overshoot, and edge distortion, are subsequently characterized by the local predistortion model.

Based on the aforementioned first-order Markov assumption, the one-step transition probability from state X_i to state X_j is defined as:

$$P_{ij} = P(X_{k+1} = X_j \mid X_k = X_i), \quad (6)$$

where $i,j \in \{1, 2, \ldots, 16\}$. Since P_{ij} denotes the conditional probability of transitioning to state X_j at the next time instant given that the current state is X_i, the transition matrix satisfies $P_{ij} \geq 0$ and $\sum P_{ij} = 1$. Thus, P is a row-stochastic matrix, and its i-th row completely characterizes the possible state transitions and their corresponding probability distribution starting from state X_i.

2.2. State Transition-Dependent Transient Distortion Modeling

The aforementioned Markov model characterizes the statistical evolution of the discrete state sequence in a multi-level ADTx, whereas its transient nonlinear distortions primarily occur within localized time intervals associated with state transitions. During PWM modulation, the branch state sequence is jointly constrained by the carrier-phase relationships and variations in the input signal. Different state transitions therefore correspond to different binary state combinations and state-change characteristics, potentially resulting

in different transient responses. Consequently, the state-transition probability alone is insufficient to characterize the actual distortion risk associated with different state transitions. It is therefore necessary to further establish the relationship between state transitions and localized transient distortions, and to quantitatively evaluate the importance of different state-transition paths by jointly considering their occurrence probabilities, state-change characteristics, and transient distortion levels.

The state-transition process is defined as T_{ij}:$X_i \rightarrow X_j$, where $X_i = X_k$ denotes the current state and $X_j = X_{k+1}$ denotes the state at the next time instant. The corresponding state-change magnitude is defined as:

$$\triangle X_{ij} = X_j - X_i, \tag{7}$$

where $\Delta X_{ij} \in \{-1, 0, 1\}^4$ denotes the change direction of each state component during the transition from X_i to X_j. To quantify the magnitude of the state change [18,19], the Hamming distance is introduced as:

$$d_H(X_i, X_j) = \sum_{n=1}^{4} |x_n(X_j) - x_n(X_i)|. \tag{8}$$

For an ideal five-level outphasing PWM architecture, the fixed phase offsets among the four carrier signals generally cause state-change events in different dimensions to occur at different time instants. Consequently, the system state evolution is primarily characterized by sequential state transitions involving changes in individual state components. In this case, the state vectors at adjacent time instants typically differ in only one dimension, satisfying the following condition.

$$d_H(X_i, X_j) = 1. \tag{9}$$

However, the Hamming distance only quantifies the number of state components that change during a state transition and cannot further distinguish the response differences associated with different state components and transition directions. For example, the state transitions $[1, 1, 1, 0]^T \rightarrow [1, 1, 0, 0]^T$ and $[0, 0, 0, 1]^T \rightarrow [0, 0, 1, 1]^T$ both satisfy $d_H(X_i, X_j) = 1$, but correspond to different transition directions. The former represents a $1 \rightarrow 0$ transition in the third state component, whereas the latter represents a $0 \rightarrow 1$ transition in the third state component. Therefore, the Hamming distance alone cannot distinguish between these two state transitions with different transition directions. Furthermore, in practical systems, different state components may exhibit distinct dynamic responses, resulting in significantly different transient error characteristics for different state transitions.

Previous research on pulse-distortion modeling and compensation in all-digital transmitters primarily addressed waveform distortions associated with pulse edges [18]. Although this approach provided an important foundation for understanding switching-induced nonlinearities, the transient behavior of a practical multi-level ADTx can also be affected by propagation-delay mismatch, amplitude imbalance among switching branches, and transient overshoot. These nonidealities may produce different error responses depending on the underlying switching-state transition path.

Building upon the previously investigated ADTx architecture, the present work considers four major distortion mechanisms: delay mismatch, edge distortion, amplitude imbalance, and transient overshoot. Rather than treating these effects solely as output waveform errors, the proposed model associates their combined transient responses with individual state-transition paths. This formulation provides the basis for the subsequent Markov state-transition-aware importance evaluation and selective FIR compensation.

Therefore, the transient nonlinear distortion in a multi-level ADTx cannot be characterized solely by the transition of the final output level and should instead be modeled as a state-transition-path-dependent function.

$$e(k) = F(T_{ij}). \tag{10}$$

The same output-level transition may result from different combinations of underlying binary switching states, while different switching-state combinations correspond to different branch switching processes and transient responses. Consequently, the transient distortion should be further modeled as a state-transition-dependent distortion function associated with the specific switching-state transition.

Considering the major hardware nonidealities, including amplitude error, delay mismatch, overshoot, and edge distortion, the total transient error associated with the state-transition path T_{ij} can be expressed as:

$$e_{ij}(t) = e_{amp,ij}(t) + e_{delay,ij}(t) + e_{over,ij}(t) + e_{edge,ij}(t). \tag{11}$$

Here, e_{amp} denotes the amplitude imbalance error caused by unequal gains among the power-amplifier branches. This error introduces amplitude deviations before and after state transitions. The term e_{delay} represents the delay-mismatch error resulting from unequal propagation delays among the switching branches, which may introduce phase perturbations. The term e_{over} denotes transient overshoot caused by differences in the dynamic responses of the power-amplifier branches during level switching. Finally, e_{edge} represents pulse-edge distortion associated with gate-level timing errors and the charging and discharging effects of parasitic capacitances [18–20].

For the n-th state dimension, a unified damped-oscillatory transient response model is established for an arbitrary state transition $i \to j$. This model characterizes the transient distortion caused by dynamic nonidealities during state changes and captures the error-response characteristics associated with level switching.

$$e_{ij}^{(n)}(t) = \triangle X_{ij}\left[A_{ij}^{(n)} e^{-\alpha_{ij}^{(n)}(t-t_{ij})} + B_{ij}^{(n)} e^{-\alpha_{ij}^{(n)}(t-t_{ij})} \cos(\omega_{ij}^{(n)}(t-t_{ij}))\right] u(t-t_{ij}), \tag{12}$$

where ${e_{ij}}^{(n)}(t)$ denotes the transient distortion response generated during the state transition $i \to j$, and t_{ij} denotes the occurrence time of the state transition. The unit-step function $u(\cdot)$ ensures that the transient distortion response is activated only after the state transition occurs. The vector ΔX_{ij} represents the state-change vector associated with the transition, characterizing different state-transition patterns and their corresponding transition directions. The parameter ${A_{ij}}^{(n)}$ is the exponentially decaying error coefficient, primarily representing the low-frequency distortion components caused by amplitude imbalance and equivalent delay errors. The parameter ${B_{ij}}^{(n)}$ is the oscillatory error coefficient, characterizing high-frequency transient distortion components such as overshoot. The parameter ${\alpha_{ij}}^{(n)}$ is the decay factor that determines the recovery rate of the transient distortion response. The parameter ${\omega_{ij}}^{(n)}$ is the oscillation angular frequency, reflecting the oscillatory characteristics induced by parasitic effects, finite bandwidth and other dynamic nonidealities in the system.

Considering the combined effects of all state dimensions on the state-transition process, the resulting transient distortion error associated with a state transition can be expressed as:

$$e_{ij}(t) = \sum_{n=1}^{4} e_{ij}^{(n)}(t). \tag{13}$$

As indicated by (11) and (12), different state-transition paths are associated with different parameter sets $\{A_{ij}^{(n)}, B_{ij}^{(n)}, \alpha_{ij}^{(n)}, \omega_{ij}^{(n)}\}$. Therefore, even when the Hamming distance $d_H(X_i, X_j) = 1$ is identical, the corresponding transient error responses may differ in amplitude, duration, and spectral characteristics. Moreover, since $e_{ij}(t)$ occurs primarily in the vicinity of state-transition instants, it is approximately zero during stable-level intervals $e_{ij}(t) \approx 0$.

The proposed model captures transition-path-dependent distortion by incorporating internal binary switching states and transition-specific transient-response parameters. Unlike conventional behavioral models and the pulse-distortion approach in [18], it accounts for the combined effects of delay mismatch, amplitude imbalance, edge distortion, and overshoot. This formulation provides the basis for the importance evaluation and selective FIR compensation developed in Section 3.

3. Markov State-Aware Adaptive Transition Compensation Method

The Markov State-Aware Adaptive Transition Compensation Method proposed in this section is developed for the multi-level ADTx system illustrated in Figure 2. Specifically, the method is applied to the internal binary switching-state transitions of the parallel power branches. The transient distortions are generated due to amplitude mismatch, delay skew, overshoot and edge distortion. The proposed method monitors the state evolution of the multi-level ADTx and identifies critical transition paths using the Markov state-transition model. Transition-specific FIR compensation kernels are then selectively activated to directly compensate for the distortion-generation process illustrated in Figure 2.

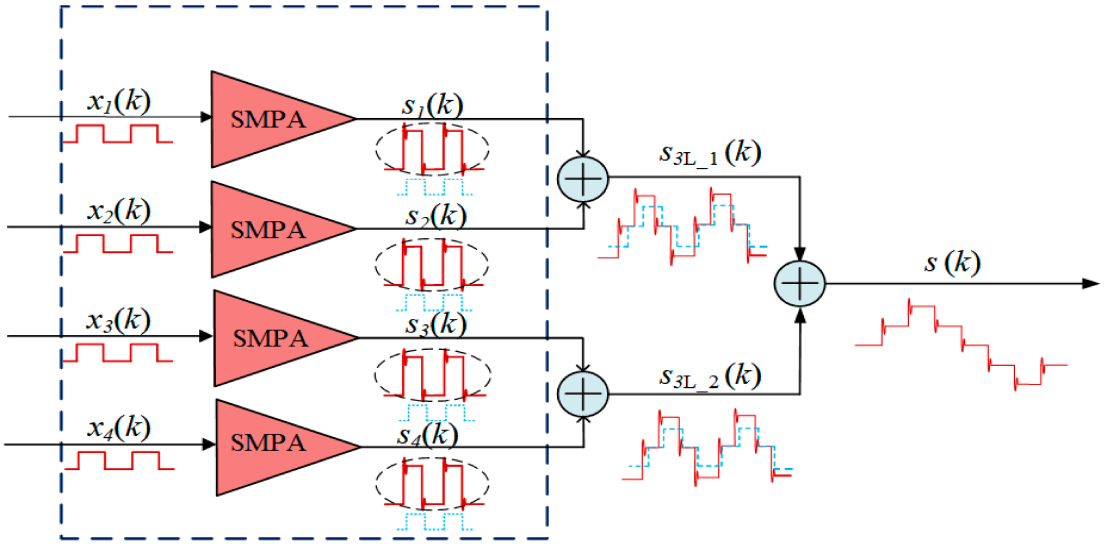


Figure 2. Illustration of the major transient distortion mechanisms in the multi-level ADTx, including propagation-delay mismatch, edge distortion, amplitude imbalance, and overshoot, based on the transmitter architecture investigated in [18].

To provide a more intuitive understanding of how the proposed method operates within the multi-level ADTx, a simplified implementation framework is shown in Figure 3. As illustrated, the proposed method consists of two stages: offline training and online compensation. In offline training, state-transition statistics are obtained, and a library of transition-specific compensation kernels is established. During online compensation, critical transition events are detected in real time, and the corresponding FIR kernels are selectively activated as needed.

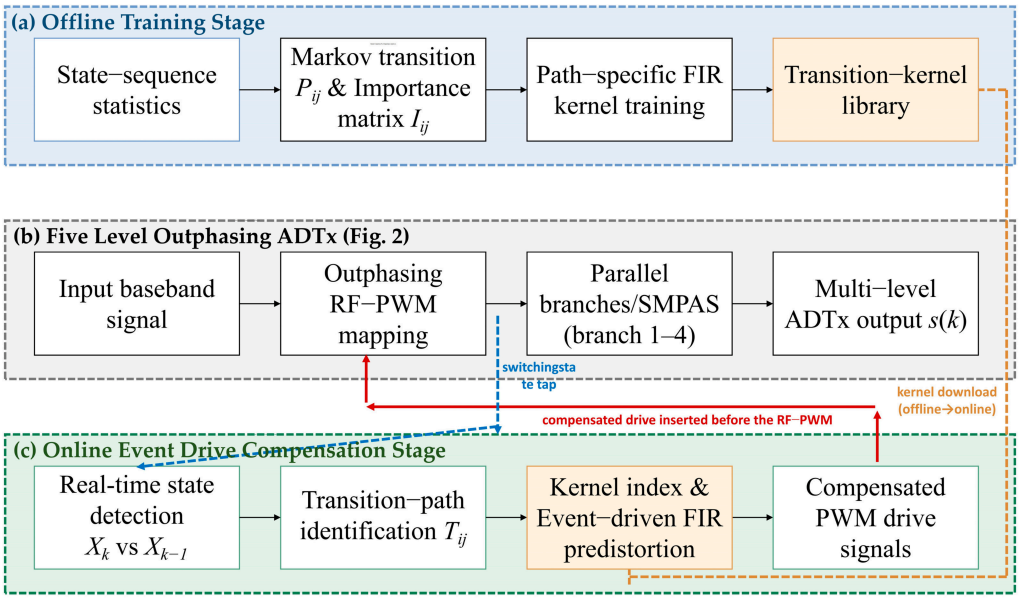


Figure 3. Simplified framework of the proposed Markov state-transition-aware event-driven compensation method applied to the five-level outphasing ADTx. (**a**) Offline training stage; (**b**) Five-level outphasing ADTx architecture corresponding to Figure 2; and (**c**) Online event-driven compensation stage.

In a multi-level ADTx, the discrete state corresponding to the output RF waveform can be represented by a four-dimensional binary state vector. During PWM modulation, state evolution is jointly constrained by the carrier-phase relationships and variations in the input signal. Consequently, the states at adjacent sampling instants are not completely independent but exhibit significant temporal correlation. Therefore, the state sequence over consecutive sampling instants can be represented as $\{X_k\}$, and its dynamic evolution can be characterized using a finite-state Markov model.

3.1. Markov State-Transition Prediction Model

According to the four-dimensional binary state vector defined in Section 2, $X_k = [x_1(k), x_2(k), x_3(k), x_4(k)]^T$, the state space contains 16 possible discrete states, denoted by $X = \{X_1, X_2, \ldots, X_{16}\}$. For any two consecutive sampling instants, the state-transition process is defined as T_{ij}:$X_i \rightarrow X_j$, where X_i and X_j denote the system states at the current and next sampling instants, respectively. Under the first-order Markov assumption, the state at the next sampling instant depends only on the current state.

$$P_{ij} = \frac{N_{ij}}{\sum_{j=1}^{16} N_{ij}}. \tag{14}$$

Accordingly, a 16 state-transition probability matrix is constructed as:

$$P = \begin{bmatrix} P_{1,1} & P_{1,2} & \cdots & P_{1,16} \\ P_{2,1} & P_{2,2} & \cdots & P_{2,16} \\ \vdots & \vdots & \ddots & \vdots \\ P_{16,1} & P_{16,2} & \cdots & P_{16,16} \end{bmatrix}. \tag{15}$$

The resulting matrix characterizes the statistical evolution of the discrete states within the five-level ADTx over time. Furthermore, the steady-state distribution

$\pi = [\pi_1, \pi_2, \ldots, \pi_{16}]$ is obtained by solving $P^{\mathrm{T}}\pi = \pi$, $\Sigma\pi_i = 1$. Here, π_i denotes the long-term probability that the system occupies state X_i.

Due to the deterministic carrier-phase relationships in the five-level outphasing PWM architecture, not all of the 256 theoretically possible state transitions can actually occur. Consequently, the state-transition matrix exhibits a pronounced sparse structure, with only a limited number of transition paths having nonzero or relatively high probabilities. This sparsity provides a theoretical basis for selectively identifying and compensating critical state-transition paths in the subsequent design.

3.2. State-Transition Path Importance Evaluation

As discussed in Section 2.2, transition probability and Hamming distance alone are insufficient to characterize path-dependent distortion. Therefore, a transition-importance metric is introduced to jointly account for transition probability, state-change magnitude, and steady-state probability.

The Hamming distance between state vectors is further introduced to characterize the magnitude of state changes, where d_{H} denotes the number of state dimensions that change during the transition. A larger Hamming distance indicates that more state dimensions are involved in a single state transition and, consequently, that the associated transient disturbance is generally more significant. By jointly considering the state-transition probability, state-change magnitude, and long-term state residence probability, the state-transition path importance metric is defined as:

$$I_{ij} = w_1 P_{ij} + w_2 \frac{d_H(S_i, S_j)}{4} + w_3 \pi_i, \tag{16}$$

where w_1, w_2, and w_3 are weighting coefficients. The first term reflects the occurrence frequency of a state-transition path during the actual modulation process. The second term characterizes the potential disturbance magnitude associated with the number of state dimensions involved in the transition. The third term represents the importance of the source state in the long-term operation of the system.

Based on the above definition, a 16×16 importance matrix I can be obtained, providing a unified evaluation of all 256 theoretically possible state-transition paths. To avoid constructing compensation models for all theoretical state transitions, the effective transition paths are further selected according to the state-transition importance matrix I_{ij}. Based on the sparse transition matrix described in Section 3.1, the effective state-transition set is defined as $\Omega = \{T_{ij} \mid P_{ij} > 0\}$. This set excludes transitions that do not occur during the observed modulation process.

3.3. Path-Specific FIR Compensation Kernel Design

Based on the path-dependent transient distortion model developed in Section 2.2, an independent FIR compensation kernel is designed for each selected transition path. For an arbitrary state-transition event T_{ij}, different transition paths may involve different state-change dimensions, transition directions, and dynamic evolution processes. Therefore, even when different paths produce the same output-level variation, their corresponding transient error waveforms may exhibit significantly different amplitudes, decay rates, and spectral characteristics. Conventional DPD methods typically employ a unified nonlinear model to compensate for continuously sampled signals as a whole, without explicitly distinguishing the local dynamic characteristics associated with different state-transition events. Consequently, they are unable to provide differentiated transient distortion compensation for different state-transition paths.

For a detected state-transition event T_{ij}, its occurrence time t_{ij} is first determined. Since the transient distortion induced by a state transition is mainly concentrated around the state-change instant, only the local response within a finite time interval before and after the transition is extracted for compensation. The state-transition observation window is defined as $[t_{ij} - T_p, t_{ij} + T_p]$, where T_p denotes the transient-response observation window and should be selected to cover the dominant duration of the transient response following the state transition. At a sampling frequency of f_s, this window corresponds to $N = 2T_p f_s + 1$, where N denotes the number of effective transient samples associated with a single state-transition event. The local error response corresponding to the transition path T_{ij} is then extracted within this window.

$$E_{ij} = \left[e_{ij}(0), e_{ij}(1), \ldots, e_{ij}(N-1)\right]^T. \tag{17}$$

Since different state-transition paths exhibit distinct transient response characteristics, an independent FIR compensation kernel is established for each effective transition path. For a given transition path T_{ij}, its compensation output is defined as:

$$\hat{e}_{ij}(n) = \sum_{l=0}^{L-1} h_{ij}(l)x(n-l), \tag{18}$$

where $h_{ij}(l)$ denotes the FIR compensation coefficient associated with the transition path T_{ij}, L is the length of the compensation kernel, and $x(n)$ represents the input digital drive signal. In matrix form, this can be expressed as:

$$\hat{E}_{ij} = X_{ij}H_{ij}, \tag{19}$$

where $H_{ij} = [h_{ij}(0), h_{ij}(1), \ldots, h_{ij}(l-1)]^{\mathrm{T}}$ denotes the compensation kernel vector associated with the state-transition path T_{ij} and X_{ij} is the convolution matrix constructed from the corresponding local input sequence. To mitigate overfitting during the training process, a regularization term is introduced into the optimization objective, and the path-specific FIR compensation kernel is obtained by minimizing the following objective function.

$$\min_{H_{ij}} J(H_{ij}) = \min_{H_{ij}} \left\|E_{ij} - X_{ij}H_{ij}\right\|_2^2 + \lambda\left\|H_{ij}\right\|_2^2, \tag{20}$$

where the second term represents the regularization constraint, which limits the magnitude of the compensation kernel coefficients and improves model stability, and λ denotes the regularization parameter. The effective state-transition paths are ranked in descending order according to their importance values I_{ij}, and the corresponding path-specific compensation kernels are established with higher priority for more important transition paths.

$$\kappa = \{(T_{ij}, h_{ij}) \mid T_{ij} \in \Omega\}. \tag{21}$$

For state-transition paths that do not occur or have extremely low occurrence probabilities, no compensation kernel is constructed. Therefore, during online compensation, the current state transition is directly identified. The corresponding compensation kernel H_{ij} is indexed to perform local predistortion. Compared with conventional global DPD methods [12,15,16], the proposed path-specific compensation mechanism does not require a unified high-order nonlinear model. Instead, it exploits the path relationships within the finite state space to characterize transient distortion, thereby enabling targeted compensation for different switching transition events.

The reliability of the offline transition kernel library depends on the representativeness of the training data and the stability of transmitter operating conditions. Insufficient

observations for rarely occurring transition paths may reduce FIR coefficient estimation accuracy. To mitigate this issue, regularized least-squares estimation is employed to improve numerical stability, while transitions without trained kernels are left uncompensated. Nevertheless, variations in temperature, supply voltage, or device characteristics may affect kernel effectiveness, indicating the potential need for periodic retraining or adaptive updating.

3.4. State-Transition-Detection-Based Event-Driven Local Predistortion Mechanism

The path-specific FIR compensation kernel library enables differentiated compensation for different state-transition events. Since transient nonlinear distortion in a multi-level ADTx is mainly concentrated around state-transition instants, continuous sample-by-sample predistortion introduces redundant computations in steady-state regions. Therefore, an event-driven local predistortion mechanism based on state-transition detection is proposed.

The real-time four-dimensional binary state vector $X_k = [x_1(k), x_2(k), x_3(k), x_4(k)]^{\mathrm{T}}$ is compared with its previous state. When $X_{\mathrm{k}} \neq X_{\mathrm{k}-1}$, a state-transition event is detected, and the corresponding transition path $T_{ij} : X_i \rightarrow X_j$ is identified. The associated FIR compensation kernel is then selected from the path-specific kernel library K as $h_{ij} = \mathrm{K}(T_{ij})$, where h_{ij} denotes the FIR compensation coefficient vector associated with the state-transition path T_{ij}. Once the corresponding compensation kernel is obtained, local predistortion is performed only within the neighborhood of the detected transition event. The compensated output can therefore be expressed as:

$$y(k) = x(k) + \sum_{m=0}^{L-1} h_{ij}(m)x(k-m), \tag{22}$$

where L denotes the length of the compensation kernel. Unlike conventional global DPD, the proposed method dynamically selects the compensation kernel according to the detected transition path rather than applying a unified nonlinear model to all samples. The online processing can be summarized as $X_k \rightarrow T_{ij} \rightarrow K(T_{ij}) \rightarrow h_{ij} \rightarrow y(k)$. Here, the state-transition matrix P_{ij} provides the prior probability information of the transition paths, while the path-importance matrix I_{ij} quantifies the compensation priority of different transition events. The path-specific compensation kernel library K then performs the actual transient-error cancelation. This structure enables the proposed method to combine state-transition awareness, path-specific compensation, and event-driven processing within a unified predistortion framework.

By restricting FIR processing to selected transition events, the proposed method reduces redundant computations during steady-state intervals.

4. Simulation Results and Performance Analysis

4.1. Implementation of the Markov State-Transition-Aware Event-Driven Compensation Algorithm

The online processing procedure of the proposed algorithm consists of four main stages: state detection, path identification, compensation-kernel indexing, and local predistortion. The state-transition probability matrix characterizes the statistical evolution of the actual state sequence, while the state-transition importance metric quantifies the relative compensation requirements of different transition paths. Based on the identified transition paths, the path-specific FIR compensation kernel library provides differentiated compensation for the corresponding transient errors. Conventional DPD applies a unified nonlinear operation to the entire input sequence. In contrast, the proposed method activates compensation only when a state-transition event is detected and selects the corresponding kernel based on the identified transition path. Consequently, the predistortion computation is concentrated in local time regions where transient distortion is most significant, thereby

avoiding unnecessary compensation during steady-state intervals. The complete online implementation procedure of the proposed Markov state-transition-aware event-driven compensation method is summarized in Algorithm 1.

This processing mechanism further enables an effective separation between offline and online computations. The Markov state statistics, steady-state distribution, state-transition importance evaluation, and path-specific FIR compensation kernels are all determined offline. Once the compensation-kernel parameters are obtained, the online process only requires current-state detection, state-transition path identification, kernel indexing, and local predistortion, without repeating state statistics, importance evaluation, or parameter training.

Algorithm 1 Event-Driven Markov State-Aware compensation With Transition Kernel Library.

Input: Discrete-time input signal $x(n)$, switching state sequence X_k
Output: Predistorted signal $y(n)$
Stage 1: Offline Training Stage
1: Collect training dataset $x(n)$, corresponding switching state sequence X_k
2: Construct discrete state space $S = \{S_1, S_2, \ldots, S_{16}\}$, according to four-channel switching states
3: Estimate Markov transition probability matrix $P_{ij} = P(X_{k+1} = S_j \mid X_k = S_i)$
4: Calculate steady-state distribution π_i
5: Calculate transition switching intensity using Hamming distance $d_H(S_i,S_j)$
6: Evaluate importance score: I_{ij}
7: Select high-risk transition events according to $\Omega = \{T_{ij} \mid P_{ij} > 0\}$
8: For each selected event $T_{ij} \in \Omega$
  8.1 Extract local transient samples corresponding to T_{ij}
  8.2 Obtain path-specific FIR kernel h_{ij} by regularized least squares
9: Construct transition Kernel Library
Stage 2: Online Event-Driven Compensation Stage
10.Initialize switching state X_0
11.for $n = 1$ to N do
12.Detect switching event $\Delta Xn = Xn - Xn - 1$
13. if $\Delta Xn \neq 0$ then
14. Identify transition event T_{ij}
15. Retrieve path-specific kernel h_i from K
16. if corresponding kernel h_{ij} exists then
17. Apply transition-specific FIR compensation
18. else
19. $y\tilde{}(n) = x(n)$
20. end if
21. else
22. $y\tilde{}(n) = x(n)$
23.end if
end for

In particular, the proposed algorithm avoids performing full DPD operations at every sampling instant during steady-state intervals. Instead, local compensation is triggered only when state-transition events are detected. This significantly reduces redundant computations and lowers the online computational complexity.

Since the number of state-transition events Ne is much smaller than the total number of samples N, i.e., $Ne \ll N$, the proposed event-driven scheme reduces the online FIR computation from $O(N^2)$ to $O(NeN)$ in Table 1.

Table 1. Computational complexity comparison.

Method	Search Strategy	Search Dimension	Evaluations	Complexity
Conventional DPD	Global sample-by-sample processing	N	N	$O(N^2)$
Proposed Method	Event-driven local processing	Ne	Ne	$O(NeN)$

The proposed method is fully implemented in MATLAB according to Algorithm 1, including state-sequence statistics, Markov state modeling, state-transition importance evaluation, path-specific compensation-kernel training, and online event-driven compensation. Figures 4 and 5 illustrate the offline state-modeling and path-specific kernel library construction, and the online event-driven compensation process, respectively. Based on these implementations, the next subsection compares the system performance before and after compensation in terms of spectral characteristics, EVM, and constellation diagrams. The results are used to evaluate the effectiveness of the proposed method in suppressing state-transition-induced transient distortion in the multi-level ADTx.

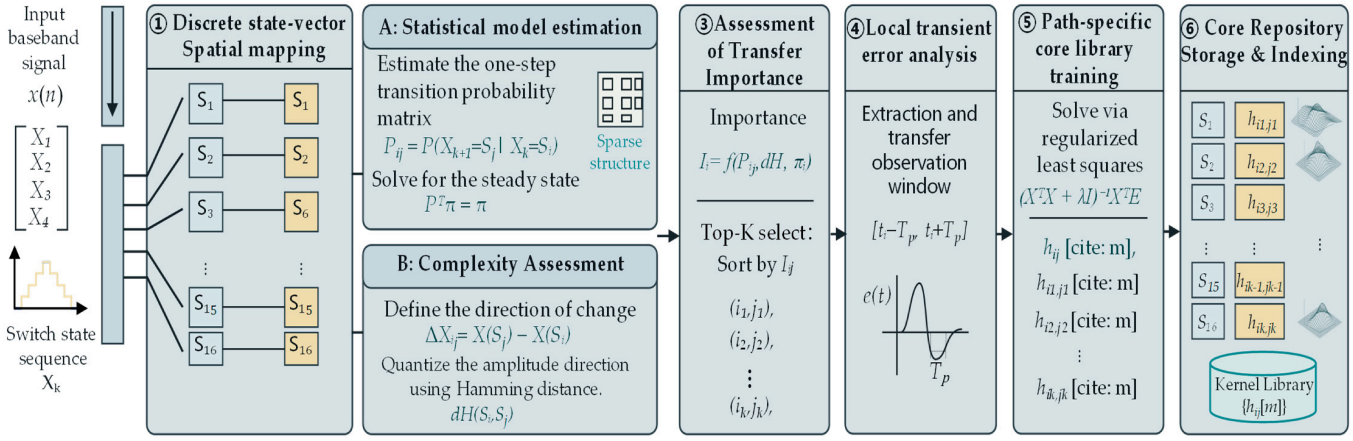


Figure 4. Workflow for offline state modeling and construction of path-specific kernel libraries.

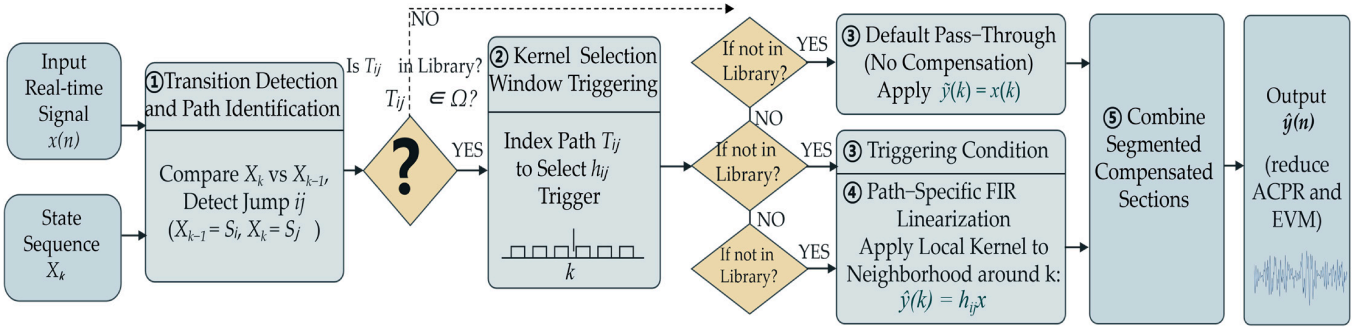


Figure 5. Online event-driven compensation procedure.

4.2. Simulation Platform and Parameter Settings

To validate the effectiveness of the proposed adaptive compensation algorithm based on Markov transition analysis and the importance matrix, a multi-level ADTx simulation platform is established in MATLAB R2024b (MathWorks, Natick, MA, USA).

At the transmitter, a 16-QAM modulated baseband signal is generated and pulse-shaped using a root-raised-cosine (RRC) filter, followed by five-level quantization and mapping. The resulting signals are applied to the multi-level ADTx architecture to generate the RF waveform, where a transition-induced transient distortion model is incorporated into the transmission path. At the receiver, the received signal is demodulated, and the system performance is evaluated in terms of the ACPR and EVM. The main simulation parameters are summarized in Table 2.

Table 2. Simulation parameters.

Parameter	Value
Modulation scheme	16QAM
Oversampling factor	100
Sampling frequency	1 GHz
Carrier frequency	10 MHz
Compensation kernel length	25
Regularization factor λ	10

To comprehensively evaluate the compensation performance, the system performance is compared under three conditions: ideal, distorted, and compensated. To verify the effectiveness of the proposed multi-level unified modeling method, a five-level outphasing ADTx experimental platform based on delay line (DDL) is built. As shown in Figure 6, the platform consists of seven main parts: PC, digital oscilloscope, vector signal analyzer, FPGA, DDL chip, y switching power amplifier (SMPA) and coupler. The PC generates baseband signals and sets experimental parameters. The FPGA implements digital logic control, while the DDL chip provides multi-channel outphasing and delay. The SMPA amplifies switching-mode signals, and the coupler realizes RF signal coupling and sampling. The oscilloscope observes time-domain waveforms and timing distortions of each branch. The vector signal analyzer captures RF metrics such as EVM and ACPR for hardware-based algorithm validation.

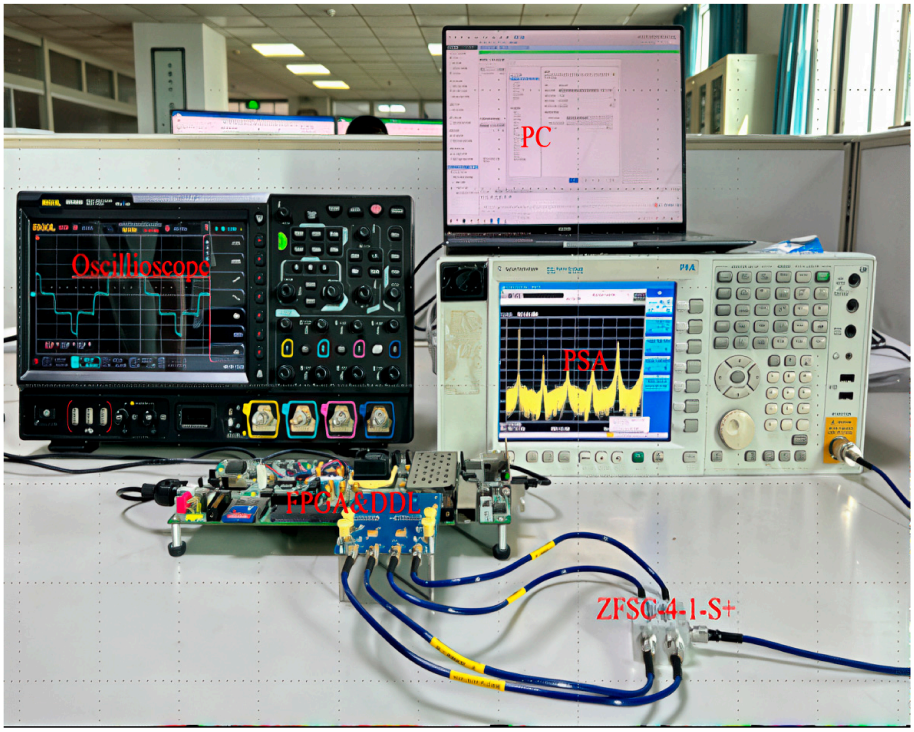


Figure 6. Five-level outphasing ADTx hardware platform.

In practical multi-level all-digital transmitters, multiple distortion mechanisms may occur simultaneously. Based on the individual distortion models, a combined model that incorporates pulse-edge distortion, overshoot, amplitude imbalance, and propagation-delay mismatch is therefore established. In the time domain, the superposition of these effects introduces irregular switching transients, amplitude deviations, and timing errors into the output waveform; in the frequency domain, it generates additional harmonic and spurious components, which further give rise to in-band spectral regrowth, an elevated adjacent-channel leakage ratio, and discrete spurs at the harmonic frequencies. To verify the proposed combined model, measured and simulated results for a five-level RF-PWM output are provided in Figures 7 and 8, respectively. As shown in Figures 7a and 8a, the constellation points of the actual output deviate from their ideal positions, and the measured EVM RMS reaches approximately 5.15%. The fundamental-frequency spectra in Figures 7b and 8b exhibit clear spectral regrowth and adjacent-channel leakage, while the harmonic spectra in Figures 7c and 8c reveal pronounced spurious components extending to the fifth harmonic near 50 MHz. The close agreement between the measured and simulated results confirms the validity of the combined distortion model.

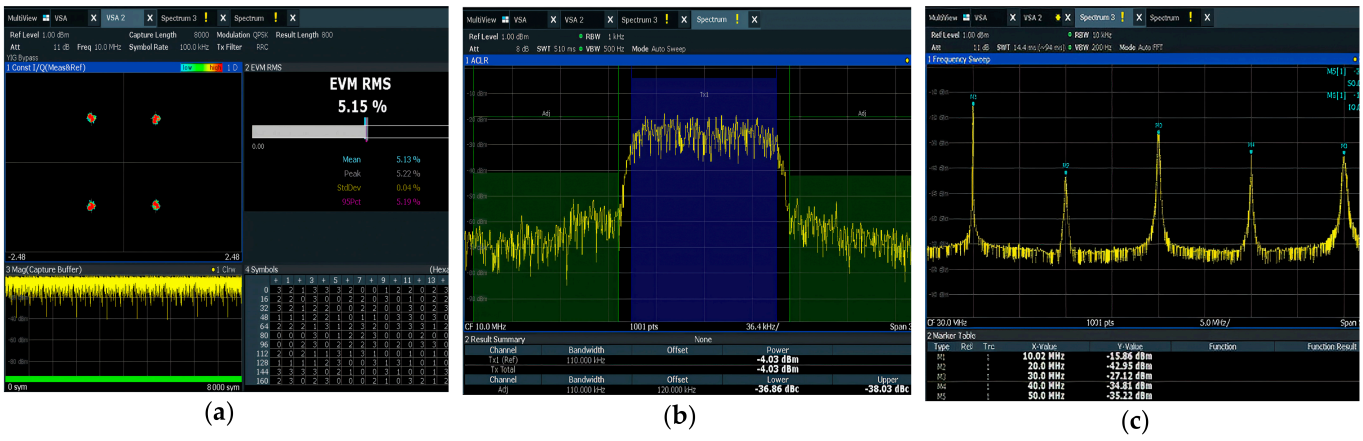


Figure 7. Measured characteristics of the five-level RF-PWM output: (**a**) EVM, (**b**) fundamental-frequency spectrum, and (**c**) fifth-harmonic spectrum.

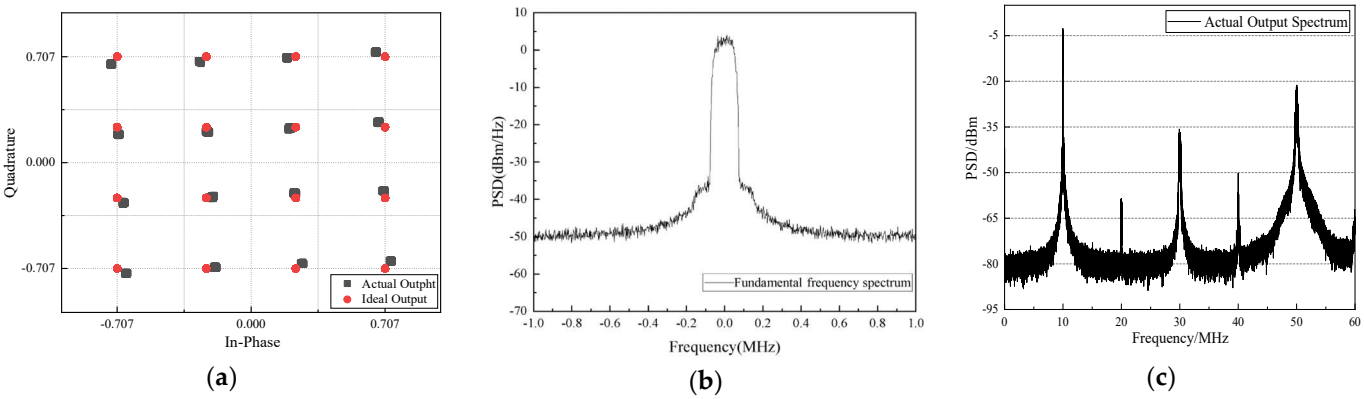


Figure 8. Simulation diagram of the five-level RF-PWM output: (**a**) EVM, (**b**) Fundamental frequency spectrum, and (**c**) fifth-harmonic spectrum.

The simulation results indicate that combined distortions can cause more pronounced signal degradation than individual distortion mechanisms. The hardware measurements provide experimental evidence of the resulting waveform and spectral impairments, supporting the physical relevance of the combined distortion model for multi-level ADTx systems.

4.3. ACPR Performance Analysis

The observed ACPR improvement can be further explained by the transition-dependent distortion mechanisms discussed in Section 2.2. Propagation-delay mismatch introduces timing deviations among switching branches, while pulse-edge distortion and transient overshoot generate additional high-frequency components around switching instants. Amplitude imbalance further modifies the combined output waveform. These effects collectively contribute to spectral regrowth and increased adjacent-channel leakage. Since the transient responses depend on the specific switching-state transitions, compensating different transition paths using their corresponding FIR kernels enables more targeted suppression of these waveform deviations.

As shown in Figure 9 and Table 3, the uncompensated ACPR of −41.32 dBc represents a degradation of 12.92 dB relative to the ideal value of −54.24 dBc. After applying the proposed compensation method, the ACPR reaches −52.93 dBc, recovering 11.61 dB of the original degradation, corresponding to approximately 89.86% of the ideal-to-distorted ACPR gap expressed in decibels. Equivalently, the adjacent-channel power ratio is reduced by approximately a factor of 14.49 compared with the uncompensated condition. The residual difference of 1.31 dB from the ideal reference indicates that the proposed method substantially suppresses the transition-induced spectral distortion, although complete elimination of the nonlinear effects is not achieved.

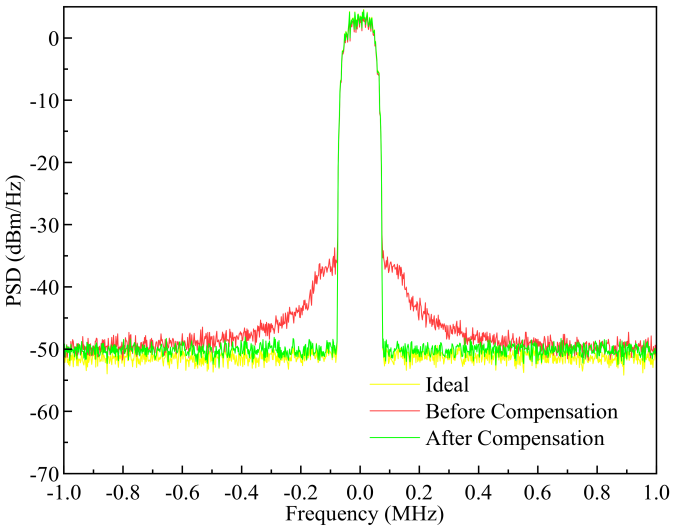


Figure 9. Baseband spectra under ideal, distorted, and compensated conditions

Table 3. ACPR performance comparison.

Condition	ACPR (dB)
Ideal	−54.24
Distorted	−41.32
Compensation	−52.93

This improvement is consistent with the proposed transition-path-aware compensation mechanism. By identifying important state transitions and applying path-specific FIR kernels within the corresponding transient intervals, the method concentrates compensation on the waveform regions associated with switching-induced distortion. The results therefore support the effectiveness of the proposed method in mitigating the combined transient distortion mechanisms under the evaluated simulation conditions.

4.4. EVM Performance Analysis

As shown in Figure 10, the uncompensated constellation points deviate noticeably from their reference positions. After compensation, the points move closer to the ideal constellation. Table 4 quantifies this change that EVM decreases from 6.02% to 1.13%, an absolute reduction of 4.89 percentage points. The residual EVM remains 0.88 percentage points above the ideal reference value of 0.25%.

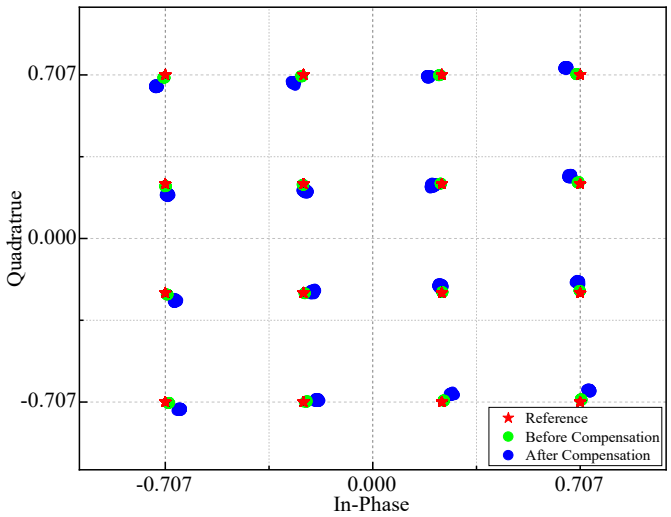


Figure 10. Constellation diagrams before and after compensation

Table 4. EVM performance comparison.

Condition	EVM
Ideal	0.25%
Distorted	6.02%
Compensation	1.13%

The spectral and constellation results provide complementary assessments of the proposed compensation strategy. The EVM results complement the spectral analysis in Section 4.3, indicating improved modulation accuracy after compensation. However, residual distortion remains relative to the ideal reference. Thus, the compensated signal approaches, but does not fully reach, the ideal performance in either metric.

The remaining differences indicate that some distortion persists after localized compensation. The event-driven strategy is intended to limit FIR processing to selected transition neighborhoods rather than continuously filter the entire sequence. Accordingly, the reported ACPR and EVM improvements establish the signal-quality benefit under the evaluated MATLAB conditions; the computational advantage should be assessed separately using measured FIR operation counts, kernel memory, and compensation-event coverage.

4.5. Comparative Performance and Complexity Analysis

To evaluate the performance and computational efficiency of the proposed method, a comparative study is conducted against the previous pulse-distortion compensation approach [18], global FIR, and full-path FIR compensation. All methods are evaluated under the same transmitter configuration and distortion conditions. The comparison considers EVM, ACPR, FIR multiply–accumulate (MAC) operations, compensation-kernel memory requirements, and compensation-event ratios. The results are summarized in Table 5.

Table 5. Performance and complexity comparison of different compensation methods.

Method	EVM (%)	ACPR (dBc)	MAC	Memory (B)	Compensated Events (%)
Uncompensated	6.02	−41.32	-	-	-
Previous work [18]	2.90	−48.36	6,400,000	1536	100
Global FIR	3.78	−49.34	3,200,000	256	100
Full path FIR	1.98	−51.31	44,798,460	5920	100
Proposed method	1.13	−52.93	2,366,700	1280	18.92

As shown in Table 5 and Figure 11, the proposed method achieves an EVM of 1.13% and an ACPR of −52.93 dBc, outperforming the previous pulse-distortion compensation method [18], which achieves 2.90% and −48.36 dBc, respectively. This corresponds to an EVM reduction of 1.77 percentage points and an ACPR improvement of 4.57 dB. These results suggest that transition-specific FIR kernels provide more effective correction of the path-dependent transient distortion considered in this study.

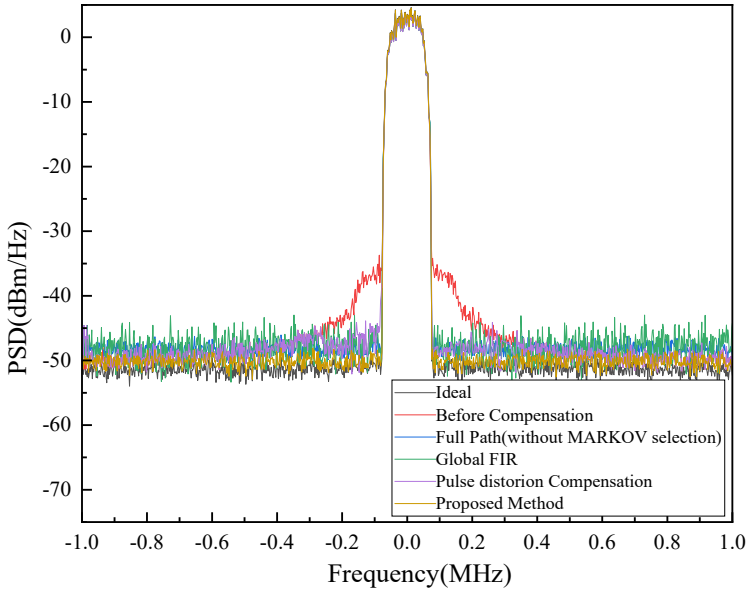


Figure 11. Power spectral density comparison of different compensation methods.

The comparative results further highlight the effects of transition-specific modeling and selective compensation. Global FIR achieves an EVM of 3.78% and an ACPR of −49.34 dBc, while full-path FIR improves these values to 1.98% and −51.31 dBc, respectively. The proposed method achieves further improvements while requiring fewer computational and memory resources. Compared with full-path FIR, FIR MAC operations and kernel memory requirements are reduced by 94.72% and 78.38%, respectively. Relative to the previous work [18], these reductions are approximately 63.02% and 16.67%. Moreover, only 18.92% of transition events require compensation. These results demonstrate a favorable balance between compensation performance and computational efficiency under the evaluated simulation conditions.

4.6. Comprehensive Performance Analysis

The improvements in ACPR and EVM indicate that the proposed method suppresses transition-induced transient distortion and reduces out-of-band spectral regrowth. The compensated spectrum and constellation diagram also approach their ideal references, confirming improvements in both spectral purity and modulation accuracy.

The comparative results in Table 5 demonstrate a favorable trade-off between compensation performance and computational complexity. Path-specific FIR kernels enable targeted correction of transient distortion associated with individual switching-state transitions. Meanwhile, the Markov-based importance evaluation identifies critical transition paths, allowing compensation to be concentrated on selected events rather than applied continuously. This selective processing mechanism reduces FIR operations and kernel memory requirements while maintaining superior compensation performance under the evaluated conditions.

Nevertheless, the observed performance depends on the accuracy of the compensation kernels and the selection of critical transition paths. Furthermore, the proposed method has been evaluated primarily through MATLAB simulations, and its real-time computational efficiency has not yet been verified through hardware implementation. Future hardware validation is therefore required to assess its practical performance.

5. Conclusions

This paper proposes a Markov state-transition-aware event-driven compensation method to mitigate transient nonlinear distortions in ADTx. The four binary switching signals of the five-level ADTx are represented using a 16-state discrete model. A first-order Markov chain is then employed to characterize the statistical evolution of the switching states.

A transition-path importance metric is developed by jointly considering transition probability, Hamming distance, and steady-state probability. Based on this metric, critical transition paths are identified for selective compensation. Path-specific finite impulse response FIR kernels are designed to compensate for transient distortions associated with individual switching-state transitions. During online operation, the corresponding compensation kernels are activated according to the detected transition events, avoiding unnecessary processing during steady-state intervals.

MATLAB simulations demonstrate that the proposed method improves ACPR from -41.32 to -52.93 dBc and reduces EVM from 6.02% to 1.13%. Although the existing hardware testbed supports the physical relevance of the modeled distortion mechanisms, the proposed compensation algorithm has not yet been validated in hardware. Future work will focus on FPGA implementation, real-time performance evaluation, and adaptive kernel updates under varying operating conditions.

Author Contributions: Conceptualization, M.W. and Z.C.; Writing—original draft preparation, M.W.; Writing—review and editing; M.W. and Z.C.; Supervision, X.Z., L.Z. and Z.W. All authors have read and agreed to the published version of the manuscript.

Funding: This research received no external funding.

Data Availability Statement: The data presented in this study are private, from the School of Electronic and Information Engineering, Nanjing University of Information Science and Technology, and The Sixty-third Research Institute, National University of Defense Technology.

Conflicts of Interest: The authors declare no conflicts of interest.

References

1. Yang, X.N.; Lou, C.Y.; Xu, J.L. *Principles and Applications of Software Radio*; Publishing House of Electronics Industry: Beijing, China, 2001.
2. Lemberg, J.; Martelius, M.; Roverato, E.; Antonov, Y.; Nieminen, T.; Stadius, K.; Anttila, L.; Valkama, M.; Kosunen, M.; Ryynanen, J. A 1.5–1.9-GHz All-Digital Tri-Phasing Transmitterwith an Integrated Multilevel Class-D Power Amplifier Achieving 100-MHz RF Bandwidth. *IEEE Solid-State Circuits* **2019**, *54*, 1517–1527. [CrossRef]

3. Hu, C.; Yin, Y.; Li, T. A Fully-Integrated Wideband Digital Polar Transmitter with 11-bit Digital-to-Phase Converter in 40 nm CMOS. *IEEE J. Solid-State Circuits* **2023**, *58*, 462–473. [CrossRef]
4. Wang, X.; Zhou, Q.; Wang, M.; Fu, H. An Outphasing Architecture Based on Parallel Radio Frequency–Pulse Width Modulation Method for All-Digital Transmitter. *Electronics* **2024**, *13*, 263–274. [CrossRef]
5. Wang, H.; Peng, C.H.; Chang, Y. A Highly-Efficient Multi-Band Multi-Mode All-Digital Quadrature Transmitter. *IEEE Trans. Circuits Syst. I Regul. Pap.* **2014**, *61*, 1321–1330. [CrossRef]
6. Madoglio, P.; Xu, H.; Chandrashekar, K.; Cuellar, L.; Faisal, M.; Li, W.Y.; Kim, H.S.; Nguyen, K.M.; Tan, Y.; Carlton, B.; et al. A 2.4 GHz WLAN digital polar transmitter with synthesized digital-to-time converter in 14 nm trigate/FinFET technology for IoT and wearable applications. In Proceedings of the 2017 IEEE International Solid-State Circuits Conference (ISSCC), San Francisco, CA, USA, 5–9 February 2017; pp. 226–227.
7. Buckel, T.; Preyler, P.; Klinkan, A.; Hamidovic, D.; Preissl, C.; Mayer, T.; Tertinek, S.; Brandstaetter, S.; Wicpalek, C.; Springer, A.; et al. A Novel Digital-Intensive Hybrid Polar-I/Q RF Transmitter Architecture. *IEEE Trans. Circuits Syst. I Regul. Pap.* **2018**, *65*, 4390–4403. [CrossRef]
8. Nuyts, P.A.J.; Reynaert, P.; Dehaene, W. A 40-nm CMOS Fully Digital Reconfigurable Transmitter with Class-D PAs Using Baseband and RF PWM. In *Continuous-Time Digital Front-Ends for Multistandard Wireless Transmission*; Springer: Cham, Switzerland, 2014; pp. 219–254.
9. Lemberg, J.; Kosunen, M.; Roverato, E.; Martelius, M.; Stadius, K.; Anttila, L.; Valkama, M.; Ryynanen, J. Digital Interpolating Phase Modulator for Wideband Outphasing Transmitters. *IEEE Trans. Circuits Syst. I Regul. Pap.* **2016**, *63*, 705–715. [CrossRef]
10. Nuyts, P.A.J.; Reynaert, P.; Dehaene, W. A fully digital PWM-based 1 to 3 GHz multistandard transmitter in 40-nm CMOS. In Proceedings of the 2013 IEEE Radio Frequency Integrated Circuits Symposium (RFIC), Seattle, WA, USA, 2–4 June 2013; pp. 419–422.
11. Yao, F.; Zhou, Q.; Wei, Z. A Novel Multilevel RF-PWM Method With Active-Harmonic Elimination for All-Digital Transmitters. *IEEE Trans. Microw. Theory Tech.* **2018**, *66*, 3360–3373. [CrossRef]
12. Morales, J.I.; Chierchie, F.; Mandolesi, P.S.; Paolini, E.E. A Distortion-Free All-Digital Transmitter Based on Noise-Shaped PWM. *IEEE Trans. Circuits Syst.* **2023**, *70*, 694–704. [CrossRef]
13. Chang, Y.C.; Chen, C.Y.; Xu, S.H.; Chen, J.H. A Low-Cost All-Digital Transmitter Using Multigigabit Transceivers. *IEEE Microw. Wirel. Technol. Lett.* **2026**, *36*, 151–154. [CrossRef]
14. Fritzin, J.; Jung, Y.; Landin, P.N.; Handel, P.; Enqvist, M.; Alvandpour, A. Phase Predistortion of a Class-D Outphasing RF Amplifier in 90 nm CMOS. *IEEE Trans. Circuits Syst. II Express Briefs* **2011**, *58*, 642–646. [CrossRef]
15. Landin, P.N.; Fritzin, J.; Van Moer, W.; Isaksson, M.; Alvandpour, A. Modeling and Digital Predistortion of Class-D Outphasing RF Power Amplifiers. *IEEE Trans. Microw. Theory Tech.* **2012**, *60*, 1907–1915. [CrossRef]
16. Hwang, T.; Azadet, K.; Wilson, R.S.; Lin, J. Linearization and Imbalance Correction Techniques for Broadband Outphasing Power Amplifiers. *IEEE Trans. Microw. Theory Tech.* **2015**, *63*, 2185–2198. [CrossRef]
17. Galaviz-Aguilar, J.A.; Vargas-Rosales, C.; Tlelo-Cuautle, E. Automated Driving of GaN Chireix Power Amplifier for the Digital Predistortion Linearization. *IEEE Trans. Circuits Syst. II Express Briefs* **2021**, *68*, 1887–1891. [CrossRef]
18. Zhu, X.; Wang, M.; Zhu, L.; Wei, Z.; Chen, Z. Modeling and Compensation of Pulse Distortion in All-Digital Transmitters. *Electronics* **2026**, *15*, 1069. [CrossRef]
19. Zhu, X.; Chen, Z.; Wei, Z.; Liu, Y.; Xu, L.; Wang, M. Analysis of Overshoot Error in 3-Level All-Digital Transmitter. In Proceedings of the 2025 IEEE 25th International Conference on Communication Technology (ICCT), Shenyang, China, 16–18 October 2025; pp. 1531–1535.
20. Wu, Y.; Chen, Z.; Huang, B.; Lu, X.; Zhu, X. Analysis of Pulse Amplitude Imbalance Error in Multi-level Outphasing All-Digital Transmitter. *Radio Commun. Technol.* **2026**, *52*, 99–106.
21. Salzenstein, F.; Collet, C. Fuzzy Markov Random Fields versus Chains for Multispectral Image Segmentation. *IEEE Trans. Pattern Anal. Mach. Intell.* **2006**, *28*, 1753–1767. [CrossRef]
22. Ghannouchi, F.M.; Hammi, O. Behavioral Modeling and Predistortion. *IEEE Microw. Mag.* **2009**, *10*, 52–64. [CrossRef]
23. Saleh, A.A.M. Frequency-independent and Frequency-dependent Nonlinear Models of TWT Amplifiers. *IEEE Trans. Commun.* **1981**, *29*, 1715–1720. [CrossRef]
24. Figueiredo, R.D. The Volterra and Wiener Theories of Nonlinear Systems. *Proc. IEEE* **1980**, *70*, 316–317. [CrossRef]
25. Ding, L.; Zhou, G.; Morgan, D.; Ma, Z.; Kenney, J.; Kim, J.; Giardina, C. A Robust Digital Baseband Predistorter Constructed Using Memory Polynomials. *IEEE Trans. Commun.* **2004**, *52*, 159–165. [CrossRef]
26. Seebacher, D.; Singerl, P.; Schuberth, C.; Dielacher, F.; Papananos, Y.; Alexiou, N.; Galanopoulos, K.; Gadringer, M.E.; Bosch, W. Predistortion of Digital RF PWM Signals Considering Conditional Memory. *IEEE Trans. Circuits Syst. I Regul. Pap.* **2015**, *62*, 2342–2350. [CrossRef]
27. Li, Y.; Wang, X.; Zhu, A. Reducing Power Consumption of Digital Predistortion for RF Power Amplifiers Using Real-Time Model Switching. *IEEE Trans. Microw. Theory Tech.* **2022**, *70*, 1500–1508. [CrossRef]

28. Zheng, N.; Yuzhong, J.; Wenliang, Z.; Gang, L.; Zhi, H. Mathematical analysis of 4-ary MSK signal spectrum based on Markov chain Process Strategy. In Proceedings of the 2021 IEEE 4th International Conference on Electronic Information and Communication Technology (ICEICT), Chongqing, China, 18–20 June 2021; pp. 1196–1201.
29. Wang, H.S.; Moayeri, N. Finite-state Markov channel-a useful model for radio communication channels. *IEEE Trans. Veh. Technol.* **1995**, *44*, 163–171. [CrossRef]
30. Shestakov, V.V.; Manonina, I.V. Mathematical Model of the Error Source of Radio Channels with Rayleigh Fading. In Proceedings of the 2023 IEEE 24th International Conference of Young Professionals in Electron Devices and Materials (EDM), Pskov, Russia, 28–30 June 2023; pp. 1–7.

Disclaimer/Publisher's Note: The statements, opinions and data contained in all publications are solely those of the individual author(s) and contributor(s) and not of MDPI and/or the editor(s). MDPI and/or the editor(s) disclaim responsibility for any injury to people or property resulting from any ideas, methods, instructions or products referred to in the content.